

# Atomic and molecular spectra emitted by normal liquid ${}^4\text{He}$ excited by corona discharge

Z.-L. Li, N. Bonifaci, and A. Denat

*G2E.lab, CNRS et Universite Joseph Fourier, Grenoble, France*

V.M. Atrazhev

*Joint Institute for High Temperatures, RAS, Moscow, Russia*

E-mail: atrazhev@yandex.ru

V.A. Shakhatov

*Topchiev Institute of Petrochemical Synthesis, RAS, Moscow, Russia*

K. von Haeften

*Department of Physics and Astronomy, University of Leicester, UK*

Received December 1, 2010

The liquid  ${}^4\text{He}$  at fixed temperature 4.2 K and different pressures up to 8 MPa was excited by corona discharge of both negative and positive polarity. Emission of He I atomic lines and  $\text{He}_2$  molecular bands are observed. In negative corona the lines spectra show a distinct blue-shift and line-broadening, which becomes stronger with the pressure increasing. The rotational structure of molecular bands is resolved at pressures (0.1–0.2) MPa. The blue shift of the Q-branch maximum at different pressures was observed. Rotational temperature of 900 K has been estimated for the  $d^3\Sigma_u^+ - b^3\Pi_g$  molecular band. A positive corona was realized on a point anode for fewer radii of the electrode and larger voltage than in the negative corona. Electric currents in both negative and positive corona differ weakly. Spectral analysis of the radiation from the positive corona shows qualitative differences of spectral features of these discharges. The spectra observed in the positive corona have marked non-symmetric shape. The asymmetric atomic and molecular spectra show an increased intensity of their long-length (red) wings.

PACS: 36.40.Mr Spectroscopy and geometrical structure of clusters;

71.35.Aa Frenkel excitons and self-trapped excitons;

**73.20.-r** Electron states at surfaces and interfaces;

**78.40.-q** Absorption and reflection spectra: visible and ultraviolet.

Keywords: spectra, liquid normal helium, corona discharge.

## Introduction

Liquid helium is a fascinating substance with many peculiarities due to its highly quantum nature. A particular special feature of liquid helium is its intense luminescence in the visible and near infrared spectral range. This luminescence has been observed from superfluid  ${}^4\text{He}$  that has been bombarded with high energetic electrons [1,2], from liquid helium excited by a corona discharge [3–5] as well as from  ${}^4\text{He}$  and  ${}^3\text{He}$  droplets that were excited by monochromatic synchrotron radiation [6–8]. The visible and

near infrared luminescence stems from transitions between electronically excited states and the reason why such radiative transitions are observed in liquid helium is its negative electron affinity. Usually, in condensed matter systems transitions between electronically excited states are fast and non-radiative. This is not the case for liquid helium because after electronic excitation the energy localizes in Rydberg-type He atoms or excimer molecules and due to the negative electron affinity a repulsive force establishes between the Rydberg electron orbital and the surrounding

ground state helium atoms. As a consequence the surrounding helium atoms are pushed away within a short time [9,10] creating a cavity around the  $\text{He}^*$  and  $\text{He}_2^*$  [11], which is often referred as a “bubble” and which has typical radii between 10 and 20 Å depending on the electron’s orbital radius [12]. Bubbles of similar type are well known to enclose electrons in liquid [13] and even dense gaseous helium [14]. Within the confinement of these cavities the perturbation by surrounding ground state helium atoms is low and the electronic life time of the excited atoms or excimers is almost similarly long as for free species in the vacuum. The remaining perturbation by the ground state helium atoms surrounding the bubble is nevertheless strong enough to cause broadening and wavelength shifts of the atomic and molecular lines and the magnitude of the widths and shift was found to depend on the applied pressure [3,15]. The hydrostatic pressure was also found to affect the line intensity distribution of the rotational spectrum of the confined  $\text{He}_2^*$  [3] as well as the total luminescence yield. For instance, at high pressures exceeding 40 bar no luminescence was observed [3].

To obtain a better understanding of these effects we have initiated a systematic spectroscopic investigation of liquid helium in a cell which is excited by a corona discharge [16,17]. The corona discharges have the potential for a relatively simple and versatile excitation source to investigate electronic excitations and luminescence in liquid helium as they allow changes over pressures and densities over a very wide range. The liquid  $^4\text{He}$  under fixed temperature 4.2 K and different pressures up to 8 MPa was excited by corona discharge on sharp tungsten tips of both a negative and a positive polarity. Emission He I atomic lines 706.8 nm and 728.1 nm and  $\text{He}_2$  molecular bands 660 nm and 640 nm has been observed and analyzed. All spectra show a distinct blue-shift and line-broadening which become stronger with increasing pressure. The rotational structure of the molecular bands is resolved at the pressures (0.1–0.2) MPa. The non-resolved profile of the bands recorded at 0.6 MPa resembles the one from [1] where superfluid helium was bombarded with high energetic electrons. Shift of the bands Q-branch maximum was studied at different pressures. The shift measured is in a good agreement with experimental data [15] obtained in superfluid He II at 1.7 K. The rotational structure of the singlet band  $\text{D}^1\Sigma_u^+ - \text{B}^1\Sigma_g^-$  (660 nm) resolved for pressures < 0.2 MPa is similar to that observed in luminescence of liquid droplet excited by synchrotron radiation [7].

The corona discharge on point anode (positive corona) was realized if a radius of the electrode was small enough, 0.45  $\mu\text{m}$ , and voltage was some larger than that in the case of the negative corona. The mobility of electrons and positive ions are close each other in LHe. Therefore, electric currents of both negative and positive corona differ weakly. However the spectral analysis of the radiation from the positive corona shows qualitative differences of spectral

features of these discharges. Both atomic lines and molecular bands were observed. The spectra observed in the positive corona have marked non-symmetric shape. The spectra show an increased intensity of their long-length wings. Such “red satellites” have been observed in the vicinity of both atomic and molecular lines. In positive corona this effect is more significant than in spectra of negative corona.

## Experiment

The experimental set up has been described elsewhere [3] and we will give only a brief summary of the main features. 99.9999% helium is extra purified by passing it through a series of cold traps and activated charcoal. The purified helium is then immersed into a high pressure cell that allows pressure variations up to 10 MPa. The cell is equipped with two windows and attached to a liquid helium bath cryostat that provides temperatures down to 4.2 K. Two electrodes were inside the cell, the first of which is a sharp tungsten tip and the second, which is a flat plate 8 mm apart from the end of the tip. The tips have been produced by electrolytic etching and had radii 0.45  $\mu\text{m}$  and 2.5  $\mu\text{m}$ . Electrodes were supported by Marcor insulators. High voltage from a dc stabilized power supply (SpellmanRHSR/20PN60) is applied to the electrodes. Light emitted from the region close to the point electrode is collected on the entrance slit of a spectrograph (SpectraPro-300i, 300 mm focal length, aperture f/4.0), equipped with 3 gratings (150 gr/mm and two of 1200 gr/mm blazed at 750 nm and 300 nm respectively). The 2D-CCDTKB-UV/AR detector is located directly in the exit plane of the spectrograph. Its dimensions are 12.3×12.3 mm with 512×512 pixels of 24×24  $\mu\text{m}$  for each pixel. In order to reduce the dark current, the detector was cooled to a temperature of 153 K (dark current < 1 e/pixel/heure at 153 K). The instrumental broadening measured by recording profiles of argon lines from a low pressure discharge lamp is  $\Delta\lambda = 0.1$  nm for a 1200 gr/mm grating.

## Results and discussion

### Current of corona discharge

Corona initiation has a threshold nature both for negative and positive polarity. For negative corona, above a threshold voltage  $V_{\text{init}}$  a mean current with a magnitude of  $10^{-12}$  A is observed in the external circuit. With voltage increasing the current varies steeply up to a value of  $10^{-8}$  A. Then a slower current growth with the voltage is recorded which corresponds to a space charge limited current regime [17]. On decreasing the applied voltage after corona initiation, the extinction of the corona current occurs at a voltage  $V_{\text{ext}} < V_{\text{init}}$ . The large difference observed between  $V_{\text{init}}$  and  $V_{\text{ext}}$  is specific to liquid helium. This hysteresis has also been observed in LHe by Goncharov *et al.* [18]. A positive corona was observed for small radius of a tip elec-

trode  $r_p = 0.4 \mu\text{m}$  only. For the positive corona  $V_{\text{init}}$  is higher than that of the negative one and it equals 4 kV compared with 0.5 kV for cathode with the same tip radius.

In the point-plane electrodes geometry, outside the region of charge generation, which is very close to the point, the field strength is too low to maintain the ionization process. Then, the charge carriers (electrons or positive ions) injected from ionization zone, move through the drift region under the action of the field. This field is modified by the space charge of the carriers. Therefore, the space-charge-limited current is a quadratic function of an applied voltage  $V$  (or  $I^{1/2}$  vs.  $V$  is a straight line) for constant mobility of the charge carrier [19]. The square root of the mean current  $I^{0.5}$  is a linear function of the applied voltage  $V$  and the  $I^{1/2}(V)$  straight line has a slope which is proportional to a mobility  $\mu$  of charge carriers [20]. Pressure dependence of the slope means that the mobility of charge carriers in liquid He depends on hydrostatic pressure. The mobility  $\mu$  of negative charge carriers, extracted from current-voltage characteristics, is very small and it cannot be related to the mobility of free electrons. Its variation with pressure  $P$  is a non-monotonous function. At first,  $\mu$  increases with  $P$ , then goes through a maximum near  $P = 1$  MPa, and finally decreases with raising pressure. These mobility values and their pressure variation show a great similarity to the results obtained from the time-of-flight method [21]. The measured  $\mu(P)$  variation can be explained by the theoretical model (see, for example, [22]) which assumes that electrons in LHe are trapped in empty cavities. The cavity is a consequence of strong exchange repulsion between the electron and He atoms. Electron moves through the normal liquid He together with its cavity. Its drift velocity is determined in the hydrodynamic regime by the Stokes' law. The cavity radius decreases with the pressure increasing. This leads to the electron mobility increasing with pressure observed for  $P < 1$  MPa. For larger pressures, the electron mobility decreases with pressure increasing due to viscosity increasing with the pressure [21]. The positive charge carrier mobility, extracted from the current-voltage characteristics of a positive corona also exhibits pressure dependence. The ionic field strength is high enough to compress the liquid into solid phase near the ion, and the ion is surrounded by "snowball" of solid helium [23,24]. The radius of the ionic snowball increases slightly with pressure growth and the mobility of positive ions trapped in the snowball decreases monotonically with pressure increasing.

In the issue of the low mobility of charges in the drift zone the electric current of corona in LHe is very small and less than that in high electron mobility liquids such as LAr [25]. Close toward tip electrode the current density increases. For corona in LAr the Joule heating by the current leads to create a region of a gaseous plasma in the ionization zone with a temperature higher than the temperature of 84 K in a bulk liquid. In the case of corona in LHe the cur-

rent density is less and we assume that the ionization zone is filled with liquid He at the temperature of 4.2 K.

### Spectra of corona discharge

The light emitted from the corona region was collected and spectra in the range 500–1080 nm were recorded. Several atomic lines and molecular bands were identified. These lines correspond to radiative transitions between excited states of  $\text{He}^*$  atoms and  $\text{He}_2^*$  excimer molecules. At low pressure the lines are sharp and their peak position match the atomic lines and molecular bands of helium from gas phase experiments. These lines are listed in Table 1. A strong background continuum from 490 to 1100 nm appears in spectra at pressures above  $P = 4.0$  MPa. Moreover, the width of the lines increases with pressure and their relative intensity decreases. No lines and bands can be observed in spectra if the pressure exceeds 5.0 MPa.

Table 1. Transitions observed in liquid helium ( $T = 4.2$  K,  $P = 0.1$  MPa).

Atomic lines		Molecular bands	
$\lambda$ , nm	Upper-Lower	$\lambda$ , nm	Upper-Lower
492.19	4d $^1\text{D}$ -2p $^1\text{P}$	462.24	$\text{J}^1\Delta_u - \text{B}^1\Pi_g$
587.56	3d $^3\text{D}$ -2p $^3\text{P}$	464.95	$\text{e}^3\Pi_g - \text{a}^3\Sigma_u^+$
706.52*	3s $^3\text{S}$ -2p $^3\text{P}$	573.49	$\text{f}^3\Delta_u (v=0) - \text{b}^3\Pi_g (v=0)$
728.13	3s $^1\text{S}$ -2p $^1\text{P}$	575.00	$\text{f}^3\Delta_u (v=1) - \text{b}^3\Pi_g (v=1)$
1083.02	2p $^3\text{P}$ -2s $^3\text{S}$	577.00	$\text{f}^3\Delta_u (v=2) - \text{b}^3\Pi_g (v=2)$
		588.70	$\text{f}^3\Pi_u^- - \text{b}^3\Pi_g$
		639.60*	$\text{d}^3\Sigma_u^+ - \text{b}^3\Pi_g$
		659.55	$\text{D}^1\Sigma_u^+ - \text{B}^1\Pi_g$
		913.61	$\text{C}^1\Sigma_g^+ - \text{A}^1\Sigma_u^+$
		918.30	$\text{c}^3\Sigma_g^+ - \text{a}^3\Sigma_u^+$

Comments: \* Features of spectra of these transitions are discussed in the present paper.

Let us consider spectra observed in negative corona discharge. Blue shift and broadening of the lines were recorded in a range of the pressure (0.1–3) MPa. Figure 1 shows normalized intensities of the atomic line at 706 nm ( $3s^3\text{S} \rightarrow 2p^3\text{P}$  transition) being broadened and shifted with increasing pressure towards smaller wavelengths (blue shift), but with no significant changes in the symmetry of the line shape. The retained symmetric character of the line allowed us to quantify the width using the magnitude of the full width at half maximum (FWHM). The magnitude of the shift was derived from the position of the maximum

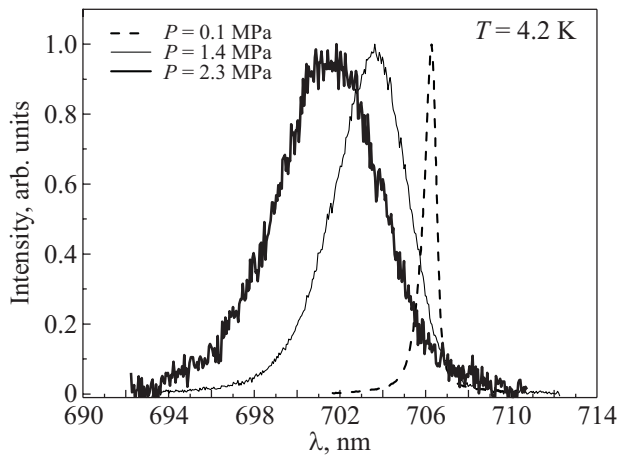


Fig. 1. Normalized intensities of the 706 nm atomic line for different pressures.

relative to line peak at 0.1 MPa. The measured shift and width of the 706 nm line are pressure dependent as shown in Figs. 2 and 3.

In a low density gas, the line profile can be accurately explained by the theory of pressure broadening [26]. Both shift and width of lines are proportional to gas density and are adequately explained by repulsive interaction between an excited  $\text{He}^*$  atom and surrounded ground state He atoms caused by the Pauli principle. The repulsion leads to blue shift. The “impact” approximation in the framework of the theory predicts strong broadening compare with shift of a line and its ratio of 7.1 [26]. Our data shows the ratio close to unity. Moreover, the calculation of the pressure broadening in helium gas at 4.2 K for different pressures and in a vapor along the liquid-gas saturated line gives more large width of the  $\lambda_0 = 706$  nm line, Fig. 3. It means that a perturbation of radiator by surrounding atoms is less than that in homogeneous gas with low density.

Previous theoretical and experimental studies have provided convincing evidence for the existence of microscopic

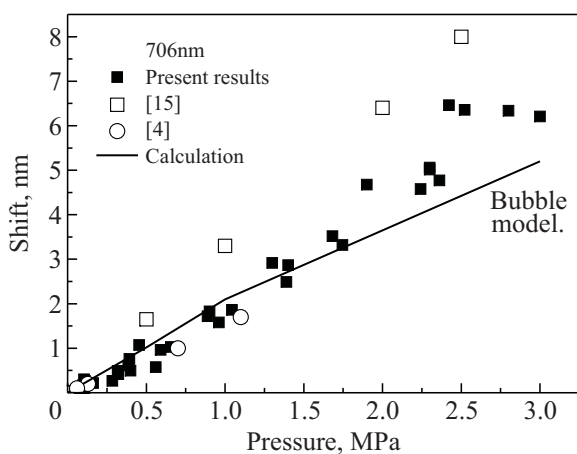


Fig. 2. Shift of 706 nm atomic line in LHe at 4.2 K for different pressures. Points — experimental data. Line — calculation in frame of “bubble” model.

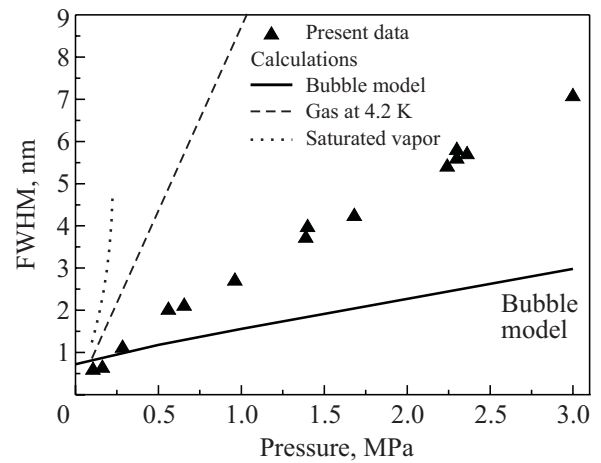


Fig. 3. Full-Width-Half-Maximum (FWHM) of the 706 nm atomic line vs. pressure. Points — experimental data. Lines — calculations.

cavities “bubble” with diameter of 1 nm surrounding excited atomic and molecular species in superfluid helium at 1.7 K [27,28]. The origin of the bubble around an excited state of atom or molecule is a balance between the repulsive interaction  $E_{\text{int}}$  between a closed shell He atoms and the Rydberg electron of  $\text{He}^*$  and the pressure  $pV_b$  and the surface tension  $\sigma S_b$  of liquid. The medium is then not homogeneous around the excited atom and the theory of the pressure broadening is not valid. The shift of the spectral lines and their width depend on the size of the bubble which is pressure dependent. When the bubble size decreases with pressure the interaction between the surrounding atoms increases due to the reduction of distance between the radiator and the perturbing ground state atoms and this ultimately leads to an increase of the line width with pressure. The well-known calculation of the atomic line shape in LHe at 1.7 K has been published in [28]. We carried out such calculations for conditions of our experiments at 4.2 K using the same simple model with a spherical bubble of radius  $R_b$  and a trial function  $n(R)$  [29,30] of a “soft” profile of its boundary

$$n(R) = \begin{cases} n_{\text{He}}[1 - (1+x)e^{-x}], & x = \alpha(R - R_b) \geq 0 \\ 0, & x < 0 \end{cases} \quad (1)$$

Here  $n_{\text{He}} = 2.2 \cdot 10^{22} \text{ cm}^{-3}$  is the number density of the liquid helium and the parameter  $\alpha$  was chosen as  $1 \text{ \AA}^{-1}$ . Because of a reduction of the surface tension a contribution of the “kinetic” term [29] in the energy balance is important

$$E_{\text{tot}} = E_{\text{int}}(n(R)) + p \frac{4\pi R_b^3}{3} + 4\pi\sigma R_b^2 + E_{\text{kin}}(n(R)). \quad (2)$$

The term was calculated using the boundary profile (1) as

$$E_{\text{kin}} = \frac{\hbar^2}{8M_{\text{He}}} \int_{R_b}^{\infty} \frac{(\nabla n(R))^2}{n(R)} 4\pi R^2 dR = 1.67 \frac{\hbar^2}{8M_{\text{He}}} 4\pi n_{\text{He}} \alpha R_b^2. \quad (3)$$

The interaction between an excited atom with surrounding atoms in the ground state was simulated using the one parameter repulsion potential  $U(R) = C_{12}/R^{12}$  with  $C_{12} = 10^{-99}$  erg·cm<sup>12</sup>

$$E_{\text{int}} = \int_{R_b}^{\infty} 4\pi R^2 \frac{C_{12}}{R^{12}} n(R) dR = 0.126 \frac{C_{12} n_{\text{He}} \alpha^{0.5}}{R_b^{8.5}}. \quad (4)$$

The total energy of the system (He\* + cavity), Eq. (2), has a minimum for an equilibrium radius of the cavity. The radius decreases from 10.6 Å at  $p = 0$  down to 8.6 Å at  $p = 3$  MPa.

The line shape  $I(\omega)$  was described in frame of the “static” approximation [31]

$$I(\omega) \propto \int_{-\infty}^{\infty} \exp \left[ i\omega\tau - 4\pi \int_{R_b}^{\infty} dR R^2 n(R) [1 - \exp(-i\tau\Delta U(R)/\hbar)] \right] d\tau. \quad (5)$$

Here  $\Delta U(R) = U_i(R) - U_f(R)$  is the difference between the interaction potentials of the excited atom in initial and final electronic states. The initial state is more extensive and its cavity has greater radius. The cavity is invariable during the radiative transition and it is larger than the equilibrium cavity for the final state of the excited atom. It allowed us to use the one parameter repulsive potential  $C_{12}/R^{12}$  in Eq. (5) and the analytical expression for the profile of the line has been obtained

$$I(\omega) \propto \int_0^{\infty} e^{-\text{Re}V(\tau)} \cos(\omega\tau - \text{Im}V(\tau)) d\tau. \quad (6)$$

Here  $\text{Re} V(\tau)$  and  $\text{Im} V(\tau)$  are real and imaginary parts of the phase function  $V(\tau)$

$$V(\tau) = \int_0^{\infty} 4\pi n(R) R^2 \left( 1 - e^{-\frac{i\tau C_{12}}{\hbar R^{12}}} \right) dR. \quad (7)$$

The  $\text{Im} V(\tau)$  and  $\text{Re} V(\tau)$  calculated using the cavity boundary Eq. (1) are linear and quadratic functions of the parameter  $\tau$ , correspondingly. It gives the Gaussian shape for the spectral line, Eq. (5). Its width and shift have a weak dependence of a magnitude of the interaction parameter  $C_{12}$ . We obtained with accuracy of a numerical factor that

$$\text{Shift} \propto \frac{\lambda_0^2}{2\pi c \hbar} \left[ \frac{C_{12}^5 n_{\text{He}}^5 p^{18}}{\alpha^9} \right]^{\frac{1}{23}}, \quad (8)$$

$$\text{FWHM} \propto \frac{\lambda_0^2}{2\pi c \hbar} \left[ \frac{C_{12}^4 p^{42}}{\alpha^{21} n_{\text{He}}^{19}} \right]^{\frac{1}{46}}.$$

The more strong dependence of the parameters was found of the diffuse boundary parameter of the cavity  $\alpha$  which was chosen as 1 Å<sup>-1</sup>. The results of the calculation

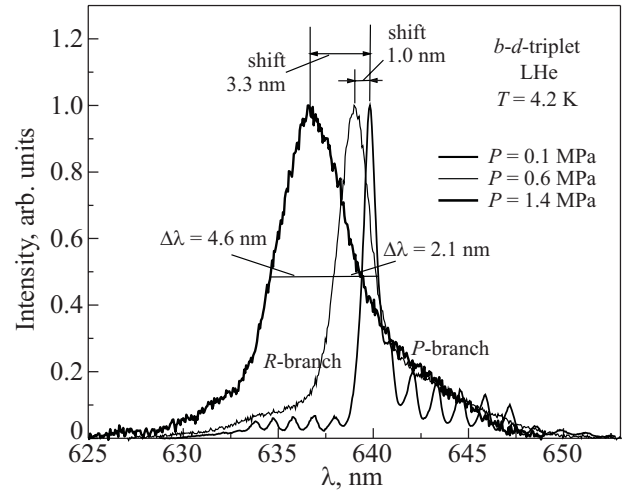


Fig. 4. Normalized intensity of molecular band  $d^3\Sigma_u^+ - b^3\Pi_g$  in LHe at 4.2 K for different pressures.

are shown in Figs. 2 and 3 as the “bubble model” lines. The calculated radii of the cavity have been founded from 10.6 Å at zero pressure to 8.6 Å at 3 MPa. The analysis showed that the ratio Shift/FWHM is a function of the parameter  $(n_{\text{He}} R_b^3)^{1/2}$  and is closed to 3 as observed in our experiment. This is strong argument confirmed the “bubble” nature of observed spectra, because the impact interaction between radiator and surrounding atoms in a gas leads to the Shift/FWHM = 0.14.

The spectral species with a structure of molecular bands have been observed in the experiments. Figure 4 shows the experimental spectrum of the  $d^3\Sigma_u^+ - b^3\Pi_g$  triplet transition. The spectrum shows (i) a distinct blue-shift and (ii) line-broadening, which become stronger with increasing pressure. At 0.6 and 1.4 MPa, individual rotational lines cannot be resolved anymore. The profile of the band recorded at 0.6 MPa resembles the one reported in [1,15] in a superfluid helium bombarded with high energetic electrons. Thus, we can conclude that, in our experiments, helium excimer molecules reside within a bubble of a diameter similar to the one reported in [15]. The  $d^3\Sigma_u^+ - b^3\Pi_g$  triplet transition is the most intense fluorescence band observed in the superfluid LHe excited by femtosecond laser pulses with intensity below a threshold of laser-induced breakdown of LHe [32]. No resolution of the rotational structure of the band was recorded in those experiments. The measurements were carried out for conditions with different temperatures from 1.4 K up to 2.8 K under saturated vapor pressures. The strong broadening (2.5 nm) central peak with red shift (2 nm) was recorded. The sign of the shift is in contradiction with our data and the results obtained in [1,15].

At pressures less than 0.2 MPa the spectrum has a well resolved rotation structure which is a subject of the numerical simulation. The upper molecular term  $d^3\Sigma_u^+$  of the transition has the rotational levels (Hund case *b*) with odd

numbers of  $K$  which is the total momentum of the molecule rotation without spin. The spin-splitting of the levels of the  $^3\Sigma$ -term of  $\text{He}_2$  molecule is very narrow [33,34] and their separation does not resolved in our measurements.

The transitions between different rotation levels are governed by the selection rule which determined three different branches of rotation lines in the molecular band such as the central  $Q$ -branch together with the  $R$ -branch in the red side and the  $P$ -branch in the blue side. Our calculations taking into account contributions of general and satellite transitions give the simple formulae for intensity of the  $Q$ -,  $P$ -, and  $R$ -branches of the rotation band

$$I_{K''}^Q \propto (2K''+1)N(K''), \quad I_{K''}^P \propto (K''+2)N(K''), \quad (9)$$

$$I_{K''}^R \propto (K''-1)N(K'').$$

Here  $K''$  is the quantum number of the upper level of the rotational transition. Honl-London factors of the  $b$ - $d$  triplet rotation lines calculated in [35,36] and listed in [37] have been used.

The analysis allowed us to estimate the population of the rotation levels using the experimental data of the rotation lines intensity. The distributions  $N(K'')$  calculated following Eq. (9) and using the measured intensities of both  $R$ -branch and  $P$ -branch lines, Fig. 4, are presented in Fig. 5 as a function of the quantum number  $K''$  of upper rotational levels. The Boltzmann distribution corresponds to a linear function in this semi-logarithmic plot. Figure 5 shows that such distribution is only exhibited for large  $K''$ . The "rotational" temperature of the distribution is 900 K, which is much higher than the temperature of the liquid of 4.2 K. It indicates that the rotating excimer molecules are far from being thermalized. Moreover, the populations derived from the  $P$ -branch intensities are larger than those calculated from  $R$ -branch intensities. This fact can formally be interpreted by the existence of an additional source of radiation that located in a range of larger wavelengths to the spectrum. The simulation of the  $d$ - $b$  spec-

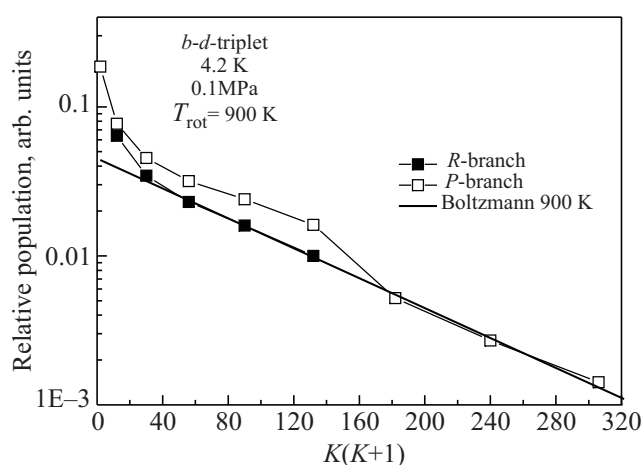


Fig. 5. Relative population of the rotational levels of the upper term  $d^3\Sigma_u^+$  (idem to Fig. 4).

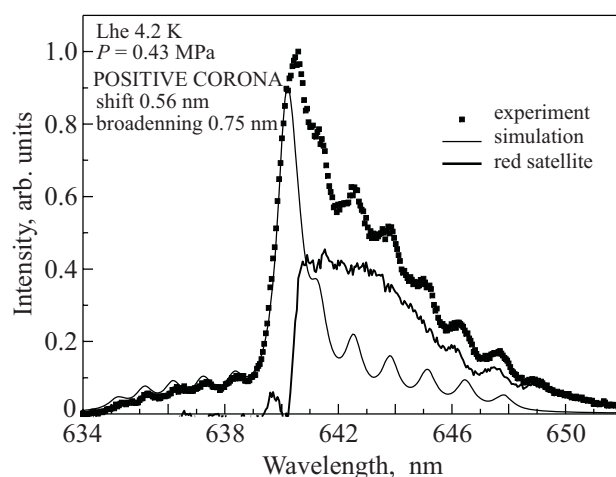


Fig. 6. Rotational spectra of transition  $d^3\Sigma_u^+ - b^3\Pi_g$  of positive corona in LHe,  $T = 4.2$  K,  $P = 0.142$  MPa.

trum shows the magnitude of the contribution of such a "red satellite" as the difference between measured and simulated spectra in the range of the  $P$ -branch lines.

The comparison of spectra observed in negative and positive corona shows that the additional radiator identified as "red satellite" presents spectral lines recorded for positive corona. Such satellites have been observed near both atomic lines and molecular bands. The phenomenon of "red satellite" is more significant in spectra recorded with positive corona discharges. The satellites were observed for both 706 nm and 728 nm atomic lines. The same "red satellites" were observed in molecular spectra and their spectrum can be shown by subtracting the simulated spectra from the measured one. The result of this procedure is presented in Fig. 6. Our calculations show that the "additional radiator" cannot be explained by contributions from higher vibration transitions such as  $(v=1, v'=1)$  which band head is located close to 642 nm. Nature of the additional radiator is unclear yet and here we can only tentatively explain the red satellite bands as possibly due to a van der Waals bound molecular complex formed by the radiating atom or molecule and single helium atom. Further calculations and experiments on the nature of the profiles of the red satellite lines and bands are in progress.

## Conclusion

We have shown that, in liquid helium at 4.2 K, the spectroscopic investigation of localized atomic and molecular excited helium states can be created by using a corona discharge as excitation source. Spectra were recorded in a large range of applied pressure from 0.1 to 4 MPa. The analysis of the observed shifts and widths show that the classical theory of line broadening (that accurately predicts the experimental line profile for helium gas at 4.2 K) cannot be applied for liquid helium. For pressures under 1 MPa the experimental width of a line is in agreement with predictions of the "bubble" theory.

For positive corona discharges in liquid helium at 4.2 K, a new phenomenon called 'red satellite' has been underscored. The "red satellite" features are tentatively assigned to the presence of an "additional radiator" of unknown origin. Further experiments and calculations are required to better understand the origin of this phenomenon.

Authors from Russia thank Russian Foundation of Basic Researches grants 08-08-00694 and 09-08-01063 for support of their work.

1. W.S. Dennis, J.E. Durbin, W.A. Fitzsimmons, O. Heybey, and G.K. Walters, *Phys. Rev. Lett.* **23**, 1083 (1969).
2. J. Keto, F. Soley, M. Stockton, and W. Fitzsimmons, *Phys. Rev.* **A10**, 872 (1974).
3. Z. Li, N. Bonifaci, A. Denat, and V. Atrazhev, *IEEE Trans. Dielectr. Electr. Insulation* **13**, 624 (2006).
4. P. Zimmermann, J. Reichert, and A. Dahm, *Phys. Rev.* **B15**, 2630 (1977).
5. V. Levitov, V. Goncharov, S. Gosteyev, T. Raskatova, V. Starobinsky, and A. Fatkin, *IEEE Transactions on Magnetism* **13**, 166 (1977).
6. K. von Haeflten, A.R.B. de Castro, M. Joppien, L. Moussavizadeh, R. von Pietrowski, and T. Moller, *Phys. Rev. Lett.* **78**, 4371 (1997).
7. K. von Haeflten, T. Laarmann, H. Wabnitz, and T. Moller, *Phys. Rev. Lett.* **88**, 233401 (2002).
8. K. von Haeflten, T. Laarmann, H. Wabnitz, and T. Moller, *J. Phys. B, At. Mol. Opt. Phys.* **38**, S373 (2005).
9. J. Eloranta and V. Apkarian, *J. Chem. Phys.* **117**, 10139 (2002).
10. M. Rosenblit and J. Jortner, *Phys. Rev. Lett.* **75**, 4079 (1995).
11. J. Hill, O. Heybey, and G. Walters, *Phys. Rev. Lett.* **26**, 1213 (1971).
12. A. Hickman and N. Lane, *Phys. Rev. Lett.* **26**, 1216 (1971).
13. J. Northby and T. Sanders Jr, *Phys. Rev. Lett.* **18**, 1184 (1967).
14. J. Levine and T.M. Sanders, *Phys. Rev. Lett.* **8**, 159 (1962).
15. F. Soley and W. Fitzsimmons, *Phys. Rev. Lett.* **32**, 988 (1974).
16. P.J. Gavin and P.V.E. McClintock, *Phys. Lett.* **43A**, 257 (1973).
17. B. Halpern and R. Gomer, *J. Chem. Phys.* **51**, 1031 (1969).
18. V.A. Goncharov and V.I. Levitov, *Izv. Acad. Nauk, Energetika i Transport (in Russian)* **12**, 134 (1975).
19. R. Coelho and J. Debeau, *J. Phys. D: Appl. Phys.* **4**, 1266 (1971).
20. N. Bonifaci, A. Denat, and B. Malraison, *IEEE Trans. Ind. Applicat.* **37**, 1634 (2001).
21. K.O. Keshishev, Yu.S. Kovdra, L.P. Mezhev-Deglin, and A.I. Shalnikov, *JETP* **29**, 53 (1969).
22. A.G. Khrapak, W.F. Schmidt, and E. Illenberger, in: *Electronic Excitations in Liquefied Rare Gases*, W.F. Schmidt and E. Illenberger (eds.), (2005) chap. 7, p. 239.
23. K.R. Atkins, *Phys. Rev.* **116**, 1339 (1959).
24. A.F. Borghesani, in: *Electronic Excitations in Liquefied Rare Gases*, W.F. Schmidt and E. Illenberger (eds.), American Scientific Publishers (2005), p. 131.
25. N. Bonifaci and A. Denat, in: *Proc. of the 12th Intern. Conf. on Conduction and Breakdown in Dielectric Liquids*, C. Mazzetti (ed.), IEEE Catalog Number 96CH35981, Roma (1996), p. 37.
26. N. Allard and J. Kielkopf, *Rev. Mod. Phys.* **54**, 1103 (1982).
27. A. Hickman and N. Lane, *Phys. Rev. Lett.* **26**, 1216 (1971).
28. A.P. Hickman, W. Steets, and N.F. Line, *Phys. Rev.* **B12**, 3705 (1975).
29. K. Hiroike, N.R. Kestner, S.A. Rise, and J. Jortner, *J. Chem. Phys.* **43**, 2625 (1965).
30. J. Eloranta, N. Schwentner, and V.A. Apkarian, *J. Chem. Phys.* **116**, 4039 (2002).
31. H. Margenau, *Rev. Mod. Phys.* **11**, 1 (1939).
32. A.V. Benderskii, R. Zadoyan, N. Schwentner, and V.A. Apkarian, *J. Chem. Phys.* **110**, 1542 (1999).
33. M.L. Ginter, *J. Molec. Spectrosc.* **18**, 321 (1965).
34. C. Focsa, P.F. Bernath, and R. Colin, *J. Mol. Spectrosc.* **191**, 209 (1998).
35. A. Budo, *Z. Phys.* **105**, 579 (1937).
36. I. Kovacs, *Rotational Structure in the Spectra of Diatomic Molecules*, Adam Higer Ltd., London (1969).
37. A. Schadee, *Communication from the Observatory at Utrecht, B.A.N.* **17**, no. 5, 311 (1964).